

Article

Influence of Different Particle Size and Rock Block Proportion on Microbial-Solidified Soil–Rock Mixture

Yongshuai Sun ^{1,*} , Ya Tuo ², Jianguo Lv ² and Guihe Wang ²¹ College of Water Resources & Civil Engineering, China Agricultural University, Beijing 100083, China² School of Engineering and Technology, China University of Geosciences, Beijing 100083, China

* Correspondence: causys666@163.com

Abstract: This paper focuses on the influencing factors of MICP solidification of soil–rock mixture. After selecting the best soil–rock ratio through screening, the MICP process is tested from two aspects of rock content and particle size. The results show that the soil–rock mixture is not a uniform carrier of the medium, and the force on the surface of the sample is not uniform. With the increase in stress load, the stress–strain curve shows a sawtooth upward trend and peak value. The microbial cemented soil–rock mixture had a particle size of 0.2–0.4 cm and 0.4–0.6 cm under the rock block proportion of 50%. The unconfined compressive strength of the microbial cemented soil–rock mixture with a rock particle size of 0.6–0.9 cm reaches the highest at 60% rock block proportion. When the rock content is 20–50%, the unconfined compressive strength decreases with the increase in particle size. When the rock content is 60%, the value of unconfined compressive strength first decreases and then increases with the increase in particle size; both SEM and XRD test results proved that *Sporosarcina pasteurii* could effectively induce the formation of calcium carbonate and crystallizes at the pores of the particles to improve the mechanical properties of the soil.

Keywords: soil–rock mixture; unconfined compressive strength; soil–rock proportion; stir and mix method; rock block proportion; rock particle size; SEM; EDS; XRD



Citation: Sun, Y.; Tuo, Y.; Lv, J.; Wang, G. Influence of Different Particle Size and Rock Block Proportion on Microbial-Solidified Soil–Rock Mixture. *Appl. Sci.* **2023**, *13*, 1325. <https://doi.org/10.3390/app13031325>

Received: 6 November 2022

Revised: 4 January 2023

Accepted: 12 January 2023

Published: 19 January 2023



Copyright: © 2023 by the authors. Licensee MDPI, Basel, Switzerland. This article is an open access article distributed under the terms and conditions of the Creative Commons Attribution (CC BY) license (<https://creativecommons.org/licenses/by/4.0/>).

1. Introduction

Soil–rock mixture is a kind of aggregate with gravel or block rock, clay, or sand as a filler. It is a special geological body with discontinuous, nonlinear, and inhomogeneous physical and mechanical properties between soil and rock mass [1]. In recent years, with the rise of various large-scale engineering construction, soil–rock mixture has been widely used as an important geotechnical engineering material due to its relatively unique physical and mechanical properties, such as wide distribution, suitable compaction, permeability, shear strength, and stability. It is an important material for the construction of slopes [2–4], tunnels [5,6], and subgrade engineering [7–9]. Due to the heterogeneity of the internal structure of the soil–rock mixture, the geological conditions are complex, and disasters such as collapses, landslides, and debris flows are prone to occur, which seriously endangers the lives and properties of the surrounding people. Therefore, it is of great significance to take appropriate measures to strengthen the soil–rock mixture to improve its bearing capacity and prevent the occurrence of such disasters.

A microbial-induced carbonate precipitation (MICP) soil reinforcement technology has been developed due to its environmental friendliness, simple process, high practical value, and low cost. It can overcome the environmental problems caused by traditional construction technology and can be used as a future environmentally friendly construction technology. It has attracted extensive attention from scholars in the field of geotechnical engineering [10–12]. MICP refers to the process of synthesizing calcium carbonate from metabolites of specific bacteria and substances in the surrounding environment. The formed calcium carbonate fills the soil pores and connects the soil and rock particles, thereby

strengthening the soil. The basic principle is that certain bacteria can produce urease during their growth, and urease can catalyze the hydrolysis of urea to produce ammonia and carbon dioxide. Ammonia and carbon dioxide can be hydrolyzed into ammonium and carbonate ions in an alkaline environment, and carbonate ions combine with calcium ions in solution to form calcium carbonate precipitates. In the field of microbial improvement of geotechnical engineering performance, the use of MICP technology to improve the physical and mechanical properties of geotechnical materials is an important topic of current research by many scholars [13–15]. The performance of soil engineering treated by MICP was significantly improved. The research includes sand [16], silt [17,18], sandy, clayey purple soil [19], yellow soil [20,21], expansive soil [22,23], mucky soil [24,25], and other types of soil. The unconfined compressive strength and anti-penetration ability of soil are significantly improved, which can be used in engineering practice. Wang et al. [26,27] also studied the influence of particle size on the mechanical behavior of geotechnical materials. Using biomineralization technology and MICP technology to improve the mechanical properties of tailings sand and fix part of the heavy metals carried by it [28–36]. It provides a new method for the economical, effective, and green scientific treatment of heavy metal ions in tailings. Microbial protection and repair technology can effectively compensate for micro-crack repair and improve the durability of concrete structures [37–43]. By filling the concrete cracks with sand and bacterial liquid, the concrete cracks are repaired, and the compressive strength of the concrete is improved, guaranteeing the stability and life of the project. The rock and soil anti-seepage plugging technology can significantly improve its permeability. MICP technology is used to conduct rock and soil plugging experiments [44–51]. It can be seen that microbial mineralization technology can form an effective plug. This method strengthens the geotechnical engineering and seepage prevention, guaranteeing its stability and durability. The particle size, particle size gradation, and relative density of soil are important factors that determine the effect of soil solidification. The academic community has carried out soil column cementation experiments for soils of various particle sizes, including kaolin, silt, fine sand, coarse sand, and gravel [44–50,52–58]. The particle size range of effective cementation is obtained through the measurement of samples with different particle size gradations [59–63]. It is found that the sand with coarser grains and suitable gradation has a better curing effect after the improvement of MICP technology. The relationship between the relative density of the soil and the cementation strength was studied [64–69], and it was found that the cementation strength of the soil was positively correlated with its relative density.

Combined with the related research of MICP, the current research focuses on the study of microbial cemented soil, and its solidification effect is often restricted and affected by many factors; however, there is a lack of research on microbial mineralization under the influence of different factors of soil–rock mixture. Based on this, this paper takes soil–rock mixture as the research object and focuses on the mechanical performance and application prospect of soil–rock mixture improved by microbial mineralization under the influence of different factors. In this paper, the prepared bacterial liquid and cementation reagent are used to mix the bacterial liquid and cementation reagent in the soil–rock mixture under different proportions. Using the unconfined compressive strength test to find the optimal ratio of soil–rock consolidation, the microbial mineralization and cementation ability and physical and mechanical properties of mixed soil–rock under the influence of rock content and particle size were discussed.

2. Microbial Improvement Test of Soil–Rock Mixture

Since the 21st century, most research still focuses on the process of bacterial influence of MICP; however, most samples are mineralized by injecting the binding solution into the plexiglass column or syringe through a peristaltic pump to prepare the sample [70,71]. These curing perfusion methods are easy to make the bacteria liquid and cementation liquid react first at the perfusion port. In addition, the sand body or loess near the water inlet is blocked by the calcium carbonate crystals formed earlier, and it is difficult for

the subsequent bacterial solution to be injected into the sample. This results in uneven cementation of the bacteria and the resulting calcium carbonate in the sample. Therefore, this experiment also carried out a new exploration of the MICP curing method using the stirring and mixing method to mix the bacterial liquid. The cementation reagent and the sample avoid the high-intensity and concentrated injection of bacterial liquid, leading to crystal blockage of the injection port, which can make the sample mix more uniform and the sample more fully cemented.

The microbial improvement test of the soil–rock mixture was carried out by using the cultivated bacterial fluid and cementation fluid. Based on the soil–rock mixture ratio, the best soil–rock ratio for microbial mineralization was selected, and the MICP process was studied from two aspects of rock content and particle size.

2.1. Bacterial Liquid

The test strain is *Sporosarcina pasteurii*, and the glycerol strains of the U.S. National Culture Bank No. (ATCC11859) were inoculated in the sterilized LB liquid culture medium. After the expansion treatment, the cells were cultured in a shaking incubator at 30 °C and 200 rpm for 30 h. The OD600 value of the activated and cultured bacterial liquid used in the paper was tested by UV (ultraviolet) spectrophotometer to 1.25. The original bacterial solution was diluted with physiological saline (0.9% NaCl aqueous solution) to meet the requirements of the experiment. According to the OD600 value of the bacterial solution and the bacterial concentration, referring to the conversion formula proposed by Ramachandran [72], the converted bacterial concentration is 11.64×10^7 cells/mL.

2.2. Cementation Reagent

The cementation reagent is the key to the reaction with the bacterial liquid, and the cementation reagent mainly contains urea and CaCl₂. Among them, urea provides nitrogen and energy sources for microorganisms, and Ca²⁺ in CaCl₂ provides calcium sources for the mineralization of microorganisms. The test cementation reagent used a urea–CaCl₂ mixture, and the molar ratio of urea and Ca²⁺ was 1:1. The concentration of the cementing solution used in this test is 0.25 mol/L; that is, the same volume of 0.25 mol/L urea solution and 0.25 mol/L CaCl₂ solution is mixed to prepare 0.25 mol/L cementing solution for later use.

2.3. Silt and Rocks

In this experiment, silt and rocks were selected as the reinforcement objects of microbial grouting. The soil used for the test was excavated at a construction site in Beijing, and the soil samples were screened by a multi-functional vibrating ballast cleaning machine. The basic physical parameters of the silt [73] are shown in Table 1. The particle size is 0–0.075 mm and 0.075–0.1 mm, the void ratio *e* is 0.54, the initial moisture content is 5%, and the plasticity index is 5.98.

Table 1. Basic physical parameters of silt.

Soil Sample Name	Particle Composition mm		Void Ratio <i>e</i>	Moisture Content <i>w</i> /%	Liquid Limit <i>w_l</i> /%	Plastic Limit <i>w_p</i> /%	Plasticity Index <i>i_p</i>	Soil Specific Gravity <i>g_s</i>	Dry Density <i>ρ_d</i>
Silt	$d \leq 0.075$ 87%	$0.075 < d \leq 0.1$ 23%	0.54	5%	21.52	15.54	5.98	2.7	1.7265

2.4. Test Plan

In order to reduce the difference in mineralization caused by the unevenness of the rocks, small-grained pebbles of uniform particle size were selected as the rocks in the soil–rock mixture. Three kinds of boulders with different particle sizes were selected: 0.2–0.4 cm, 0.4–0.6 cm, and 0.6–0.9 cm, respectively. Figure 1 shows the test silt and rocks. Five different rock content ratios were selected: 20%, 30%, 40%, 50%, and 60%, respectively. A total of 15 groups of soil–rock mixing ratio tests were carried out, as shown in Table 2.

We took the average value of three soil–rock mixture samples of the same configuration prepared for each group.



Figure 1. Raw material of soil–rock mixture: (a) silt, (b) rock.

Table 2. Mixing ratio scheme of soil and rock.

Particle Size Rock Content	20%	30%	40%	50%	60%
	0.2–0.4 cm	A1	B1	C1	D1
0.4–0.6 cm	A2	B2	C2	D2	E2
0.6–0.9 cm	A3	B3	C3	D3	E3

After the soil sample and the boulders were thoroughly mixed in proportions, the urea solution 0.25 mol/L and the CaCl_2 solution 0.25 mol/L, respectively, were prepared. We mixed urea and CaCl_2 solution to make a 0.25 mol/L cementation reagent. The moisture content of the soil–rock mixture was set to 12%, and the volume ratio of cementitious liquid to bacterial liquid was set to 1:1. We poured the cementitious liquid into the soil–rock mixture in proportion and placed it in a moisturizing bag for 6 h in order to ensure that the water molecules of the cementing solution diffused evenly in the soil and rock. To remove the air and seal the tank, after standing for 6 h, microbial grouting was carried out at room temperature (25 ± 2 °C).

The soil–rock mixture sample was prepared using a triaxial saturator, and the sample size was 39.1 mm (diameter) \times 80 mm (height). Before sample preparation, a certain soil–rock mixture sample was weighed, and a certain quality of cementitious liquid was added according to the proportion of moisture content. After stirring evenly, we sealed it with a fresh-keeping bag and placed it in a moisturizing tank for 6 h to make the calcium ions in the soil distribute as evenly as possible. Before sample preparation, 1.25 mol/L bacterial solution was mixed with the soil and rock body after 6 h of simmering in the tank. When using a triaxial saturator for sample preparation, we applied a small amount of Vaseline to the copper mold in order to reduce the friction between the sample and the cylinder wall. The sample soil–rock mass was prepared according to the quality. Each group of three soil–rock mixture samples with the same configuration was prepared. Each sample was hammered 30 times. After the last hammering, we shoveled off the soil higher than the mold, leveled the two ends of the sample, and then removed the mold vertically along the side of the sample to prevent damage and disturbance to the sample. It was loaded into the mold in five layers. The surface of the sample was flattened with a ring knife, and finally, the sample was demolded and placed at an ambient temperature of 30 °C for 5 days of

curing in a constant temperature and humidity curing box of $70 \pm 2\%$ ambient humidity. Among them, $30\text{ }^\circ\text{C}$ provides the best growth temperature for bacteria. According to the relative humidity of the China Meteorological Science Data Sharing Service Network on the official website of the China Meteorological Administration, a humidity environment of $70 \pm 2\%$ was used to simulate the underground soil humidity environment in Beijing.

In this test, manual operation was used, and the soil–rock mixture sample that had been cured for 5 days was put into a strain-type unconfined compression instrument. We adjusted the strain-type unconfined compression instrument in the uniaxial compression test. The lower compression plate (indenter) position was mainly used to test the specimen, to conduct a uniaxial unconfined compressive strength test on the sample at a uniform strain rate and a loading rate of 0.5 mm/s , and to record the data. When the sample was damaged, that is, after the inflection point of the test record data appeared, we continued the test depending on the damage of the sample. The test was stopped when the sample was damaged to a certain extent, and the corresponding data were calculated.

2.5. Microscopic Analysis of Soil–Rock Mixture Solidified by Microorganisms

Microbial mineralization is a biological reaction, and the bacteria itself have the characteristics of small size, large number, and rapid response. When the microorganisms act on the soil–rock mixture, the bacterial liquid distribution acts on the gaps between the particles, and the resulting crystals are small in size and have strong dispersibility. It is necessary to use a scanning electron microscope, SEM (scanning electron microscope), and phase analysis of X-ray diffraction, XRD, to conduct microscopic observation of the soil–rock mixture, combined with the laws of mechanical properties of the soil–rock mixture after improvement, the energy spectrum analysis and phase analysis of the samples were carried out, explore the material structure, morphology, content, distribution and other laws of microbial mineralization. The SEM was a Zeiss ZEISS-GeminiSEM 300 electron microscope. It can be magnified up to 1 million times, and very tiny material structures can be observed. The model used by the EDS spectrometer is Smartedx, and the spectrometer uses the different characteristics of X-ray-characteristic wavelengths of different elements to analyze the composition of the sample. XRD is a technique for analyzing the structure of materials by utilizing the diffraction effect of X-rays in crystalline materials. We took the broken block in the center of the soil–rock column, ground the sample finely, ground the sample to less than 200 mesh, sieved, and tested the chemical composition of the crystal in the sample by the tablet method.

3. Test Results and Microscopic Observation Analysis

3.1. Unconfined Compressive Test Results of Soil–Rock Mixture

Figure 2 shows the pictures after the uniaxial unconfined compressive strength test of the microbially cemented soil–rock mixture under different working conditions according to the table. Compression tests under the conditions of 15 groups of different particle sizes and rock block proportions are in the figure. Three samples were made for each group of samples, for a total of 45 samples. In order to reduce the data error in the experiment and observe the law more intuitively, the following are the most obvious failure modes and the average value of the experimental data under the same conditions as the basis and data support for the following figures.

By observing the failure pictures under various conditions in Figure 2, it is found that the failure forms of the samples are quite different, the crack shapes are different, and the loaded sample is sensitive to disturbance, showing certain fragmentation characteristics. Under the uniaxial unconfined compressive strength test, the failure modes of the soil–rock mixture cemented by bacteria liquid are divided into three types: tension failure, shear failure, and composite tension-shear failure. For tensile failure, the failure method is mainly to expand from the top to the bottom, and the expansion path is approximately a straight line (D1, A2, E2, A3, C3, E3). For shear failure, the failure mode is mainly a planar split along the top of the soil–rock mixed column, and the failure path basically extends diagonally. The rupture

is accompanied by local block shedding and typical shear slip surface characteristics (A1, B1, C1, E1, B2, D2). For the tensile-shear composite failure, there are obvious tension failure surfaces and shear slip surfaces. In addition, the failure crack is accompanied by local sample shedding, which is a typical composite failure mode (C2, D2, D3, B3).



Figure 2. Results of unconfined compression test of soil–rock mixture (See Table 2 for the sample corresponding to each letter).

3.2. Influence of Rock Block Proportion on Microbial-Solidified Soil–Rock Mixture

Under the condition that the concentration of bacteria liquid, the concentration of cementation reagent, and the ratio of solution remain unchanged when the rock particle size is 0.2–0.4 cm, the stress–strain values of the soil–rock mixture under different rock block proportions are shown in Figure 3. It can be analyzed from Figure 3 that the peak value of the soil–rock column with a rock block proportion of 50% is the highest, and the bearing capacity reaches the maximum at this time. The stress–strain values of the soil–rock mixture with the rock particle size of 0.4–0.6 cm under different rock block proportions are shown in Figure 4, and the peak value is also at 50% of the rock block proportion. The stress–strain curves of the soil–rock mixture with the rock particle size of 0.6–0.9 cm under different rock block proportions are shown in Figure 5, and the peak value is at 60% of the rock block proportion. The results show the following:

1. The bearing capacity of the soil–rock mixed column cemented is related to the size of the pores between the soil and rock. Due to the small particle size of the silt, it is in close contact with the rock when it is mixed, which increases the rock content and increases the pore space in the sample. *Sporosarcina pasteurii* are aerobic bacteria that increase pore space. It is conducive to the combination of bacteria and calcium ions in the cementing solution and the formation of calcium carbonate crystals on the bacterial surface film, which consolidates the surrounding soil and rocks and increases the strength of the sample.

2. The bearing strength of the soil–rock mixture is related to the amount of rock block proportion, and the strength and deformation mechanism during shearing are also different with different rock block proportions [74]. For the samples with rock content of 20% and 30%, the content of boulders is low, and the content of silt is high. During the loading process, the silt and the boulder are stressed together, the arrangement of the particles is tight due to the adjustment of the position between the particles, and the macroscopic performance is the shrinkage of the sample volume. As the small particles cohesively break down and move, the sample reaches its peak and completes the test. For the samples with rock block proportions of 50% and 60%, the content of boulder particles is high. The main reason is that large pores will appear in the sample of the block rock particles. In the initial stage of loading, the block rock is first subjected to pressure, and the silt is temporarily “protected” in the pores under the “cover” of the block rock particles. As you continue to load and increase the stress, the bonding between particles is destroyed, the pores are reduced, the particles are dislocated, and the sample volume is visually compressed.
3. In the soil–rock mixture, the silt particles are small. Under the action of loading stress, after the pores are destroyed, the bound water increases due to the shrinkage of the pores, and the bond strength between particles is reduced. As the stress increases, the volume shrinks, and the large particles re-contact to increase the bond strength again so that the sample reaches the peak value quickly, and the axial strain of the sample reaches the peak value is small.
4. During the stress loading process at a constant rate, the soil–rock mixture is not a uniform carrier of the medium, and the edges and corners of the blocks are first subjected to pressure during the loading process. The stress on the surface of the sample is uneven. With the increase in the stress load, the stress–strain curve shows a jagged upward trend and peak value.
5. It can be observed from Figure 6 that the unconfined compressive strength of the microbially cemented soil–rock mixture with the size of 0.2–0.4 cm and 0.4–0.6 cm of the boulders reaches the highest. They are 10.3 kPa and 9.6 kPa, respectively, both with a rock block proportion of 50%. The unconfined compressive strength of the microbial cemented soil–rock mixture with a particle size of 0.6–0.9 cm reaches the highest unconfined compressive strength of 9.4 kPa, with a rock block proportion of 60%.

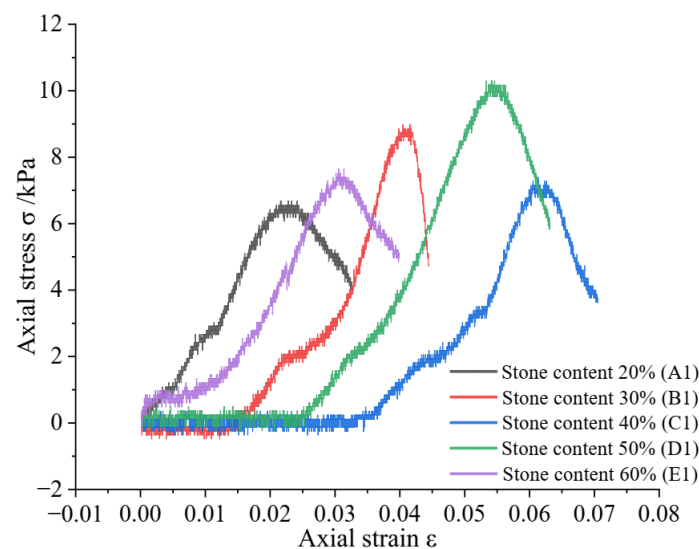


Figure 3. Stress–strain curve of soil–rock mixture stone with particle sizes of 0.2–0.4 cm.

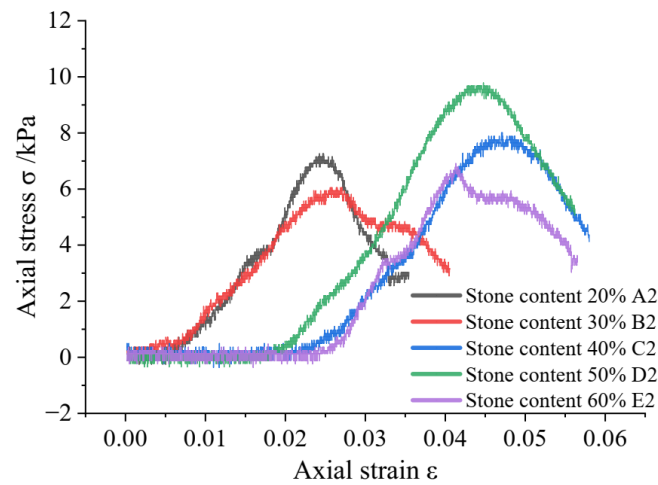


Figure 4. Stress–strain curve of soil–rock mixture stone with particle sizes of 0.4–0.6 cm.

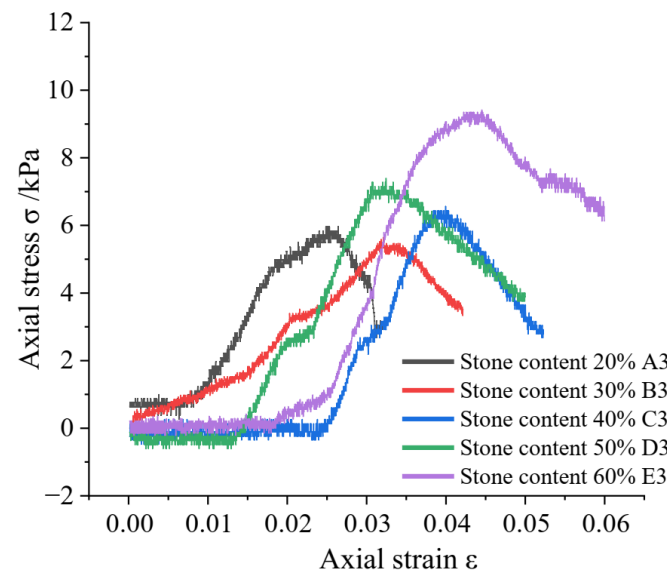


Figure 5. Stress–strain curve of soil–rock mixture stone with particle sizes of 0.6–0.9 cm.

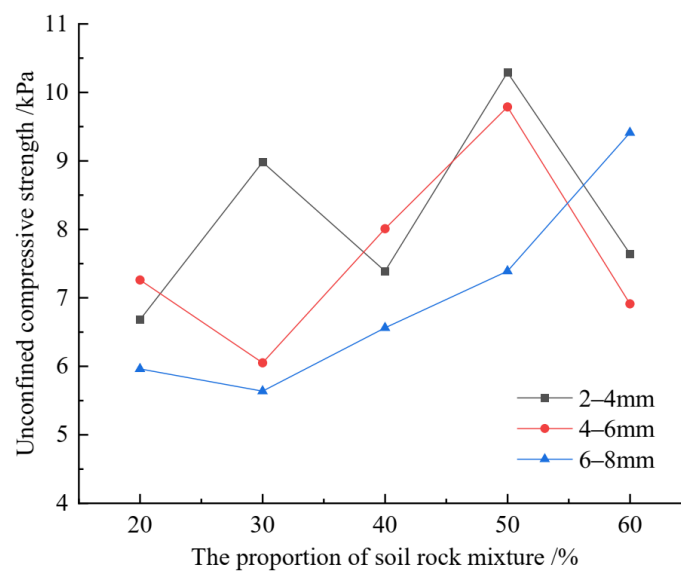


Figure 6. Unconfined compressive strength of soil–rock mixture samples with different rock content.

3.3. Influence of Rock Particle Size on Microbial-Solidified Soil–Rock Mixture

According to the analysis of the above summary, it can be seen that the cementation effect of the soil–rock mixture with 50% and 60% rock block proportion is better. It can carry a large bearing capacity, and the unconfined compressive strength is relatively suitable. Therefore, the soil–rock samples with rock content of 50% and 60% were observed separately to find out the optimal particle size ratio of the soil–rock mixture. It provides a reference for subsequent research and engineering applications. The results show the following:

1. Looking at Figures 7–9 below, under the condition that the bacterial solution concentration, cementation reagent concentration, and solution ratio remain unchanged when the rock block proportion is 50% for the soil–rock mixture with a particle size of 0.2–0.4 cm, as the sample is loaded, the stress increases with the increase in the strain. After reaching the peak, the stress gradually decreases, and the loading rate remains unchanged; therefore, the earliest maximum bearing capacity of the three particle sizes is D3–D2–D1, respectively; that is, the sample with a particle size of 0.6–0.9 cm shows a peak first, followed by a sample with a particle size of 0.4–0.6 cm, and finally a soil–rock mixture sample with a particle size of 0.2–0.4. When the rock block proportion is 60%, the earliest time for the three particle sizes to show the maximum bearing capacity is when D1, D2, and D3 show their peaks at the same time; that is, the sample with a particle size of 0.2–0.4 cm reaches the maximum bearing capacity first, and the sample with a particle size of 0.4–0.6 cm and a particle size of 0.6–0.9 cm basically has the maximum bearing capacity at the same time. The soil–rock mixture mixed with large-sized boulders has a large pore space. When compressed and squeezed, the internal pore space will be destroyed first, and the soil–rock mixture with small-sized boulders will reach the maximum bearing capacity faster than that;
2. It can be observed in Figure 9 that under the same loading rate and the same rock block proportion, in the rock block proportion of 20%, 30%, 40%, and 50%, under the same proportion of rock, the unconfined compressive strength decreases with the increase in particle size. When the rock content is 60%, the value of unconfined compressive strength first decreases and then increases with the increase in particle size. In the samples with low rock block proportion, the silt content is high, and the overall force is more inclined to the properties of silt during the loading and stressing process. During the compression process, the pores between the particles are destroyed, the bound water increases due to the shrinkage of the pores, and the bonding strength between the particles decreases, making it easier to be destroyed;
3. When the rock block proportion is low, the difference between the particle size ratio of the rock with small particle size and the soil particle size is relatively small, and it is easier to be cemented with the bacteria liquid to form a block. The compressive strength of the soil–rock mass is enhanced, so the unconfined compressive strength of the soil–rock mixture containing small-diameter rocks is higher than that of the soil–rock mixture containing large-diameter rocks under the same conditions. In the case of high rock block proportion, the large particle size of the rock and the soil particle size gap is large, and the pore space is large, giving the bacteria liquid more space for cementation and the required oxygen. At the same time, under the consolidation pressure of irregular boulders, the rocks with larger particle sizes have more particle contact points than those with smaller particle sizes. Under the loading speed of the same rate, the soil–rock mixture with large particle size is more easily broken due to the contact point, forming a stronger particle structure, and its unconfined compressive strength is greater than that of the soil–rock mixture with smaller particles.

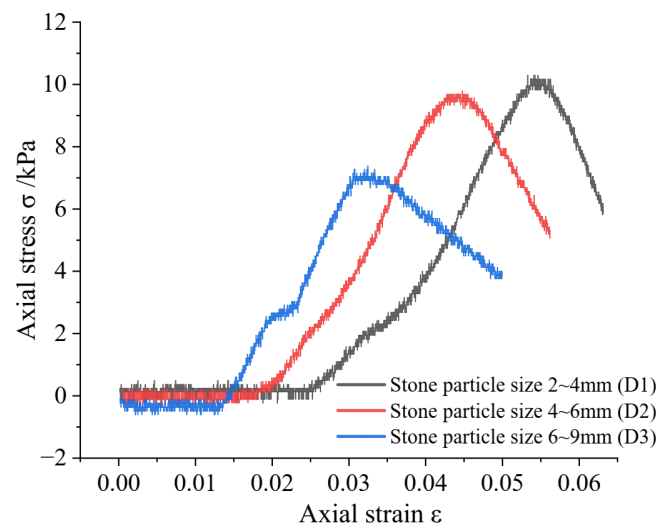


Figure 7. Stress–strain curve of soil–rock mixture sample with rock content of 50%.

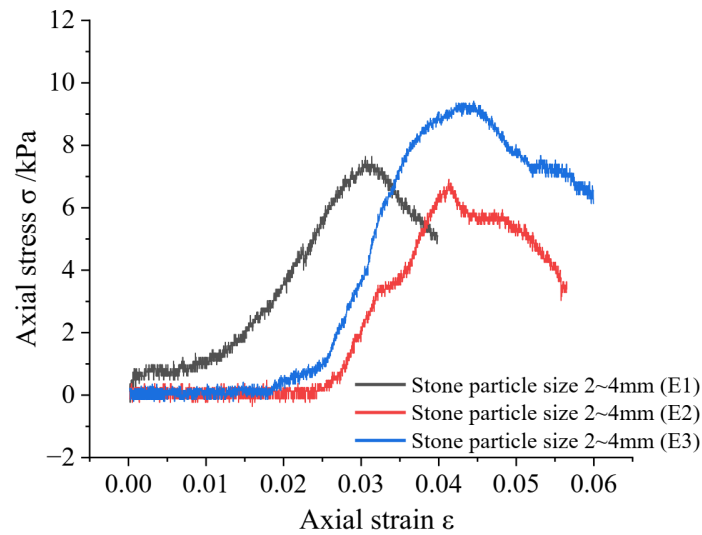


Figure 8. Stress–strain curve of soil–rock mixture sample with rock content of 60%.

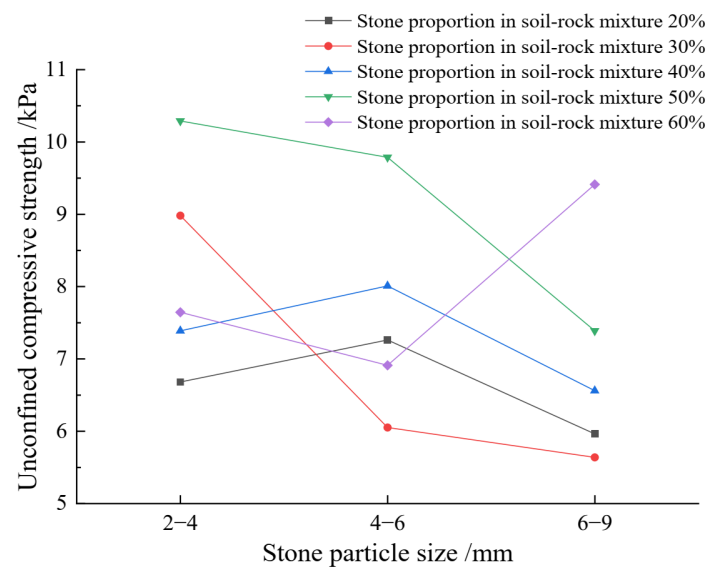
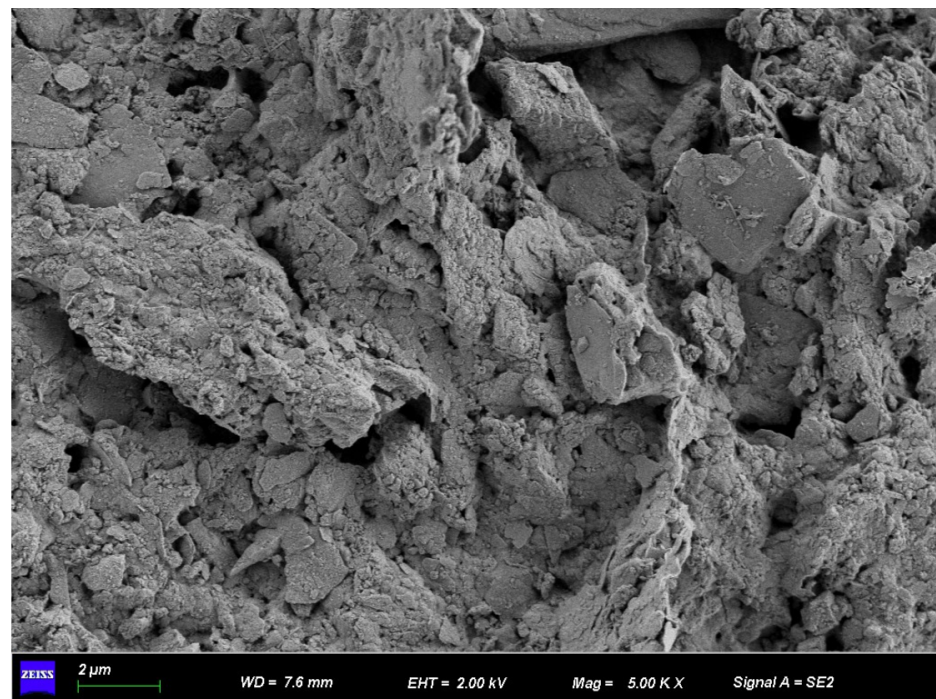


Figure 9. Unconfined compressive strength of soil–rock mixture samples with different stone particle sizes.

3.4. Microscopic Observation

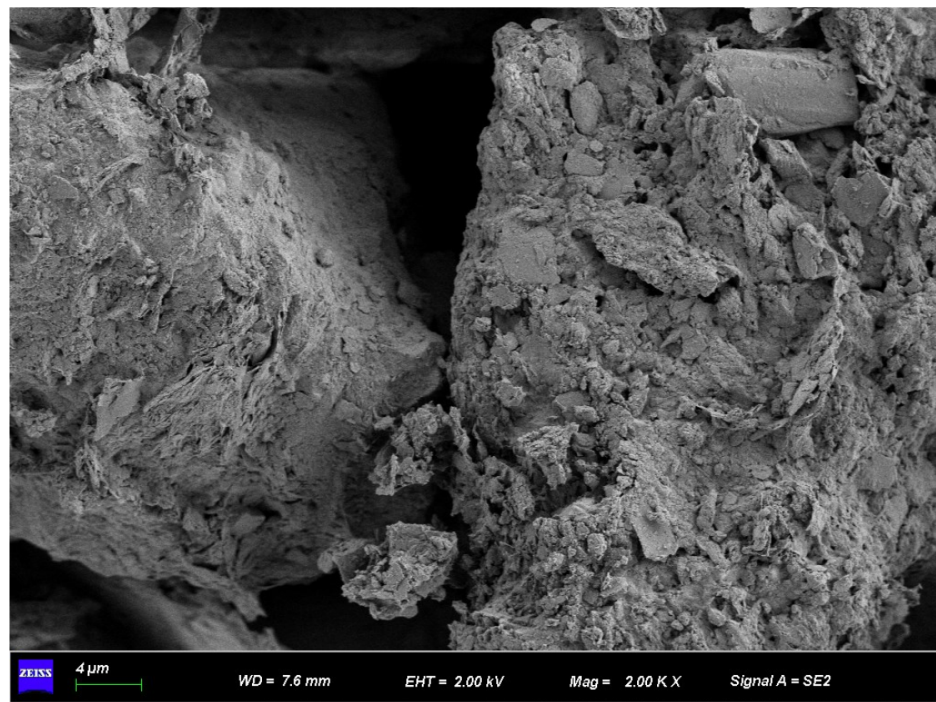
In order to better explore the mechanism of microbial mineralization in the soil–rock mixture and to feel the cementation products of microbial mineralization more intuitively, a set of blank controls was set up. In the blank control group, deionized water was used to replace the cementation reagent and bacterial liquid. Under the condition that other conditions remain unchanged, the samples were dried and then microscopically observed. D1, B3, and the blank control group were selected for microstructure and phase analysis.

Observing Figure 10, it can be observed that calcium carbonate crystals are attached to the surface of the sample, which strengthens the bonding of particles at the voids. Observing Figure 11, there are spot-like crystals on the surface of B3, which aggregate on the surface of the silt, connecting the two parts of the silt and the rock. It can be observed from Figure 12 that the surface of the sample is powdery, and there is no crystal at the connection. There is an obvious fracture failure surface in the sample, the failure contact surface is smooth, and there is no “rough feeling”, as shown in Figures 10 and 11. Observing Figure 13a, the atomic energy percentage of calcium ions in sample D1, it can be found that the percentage content of calcium ions in this sample is 0.54%, which is very small. Observing Figure 13b, the atomic energy percentage of calcium ions in sample B3 is 0.5%, compared with the atomic energy percentage of calcium ions in sample D1. Under the same mass, the calcium ion content of B3 is less than that of D1. Combined with Figure 13c, the calcium ions in the blank control group accounted for 38%, which was less than the percentage of calcium ions in D1 and B3. It is proved that the mineralization of microorganisms can indeed precipitate calcium ions between particles, which provides a theoretical basis for the mineralization of microorganisms.

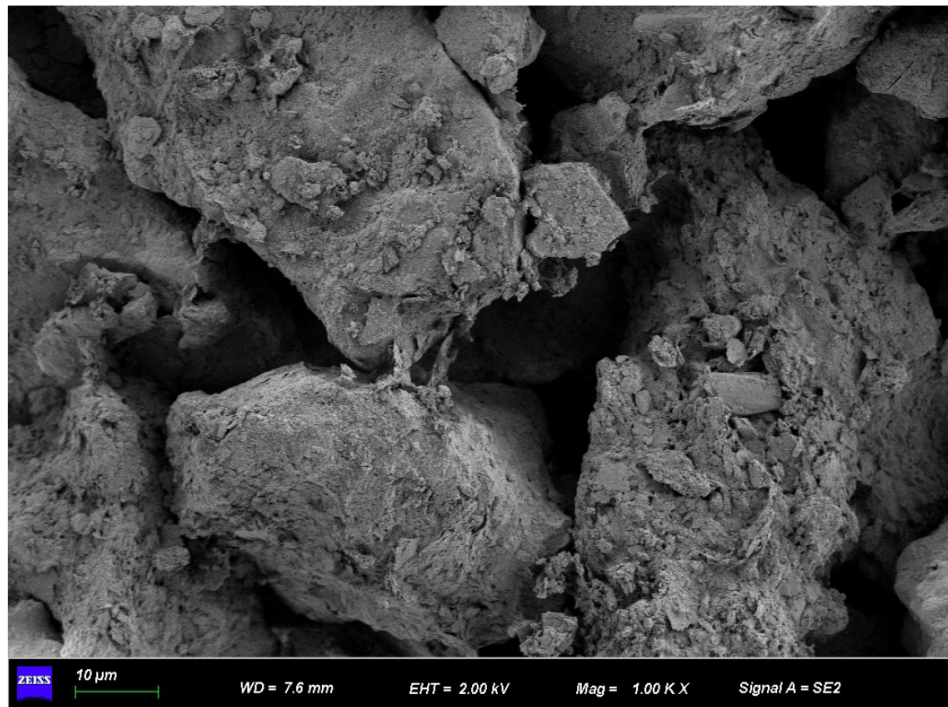


(a)

Figure 10. Cont.

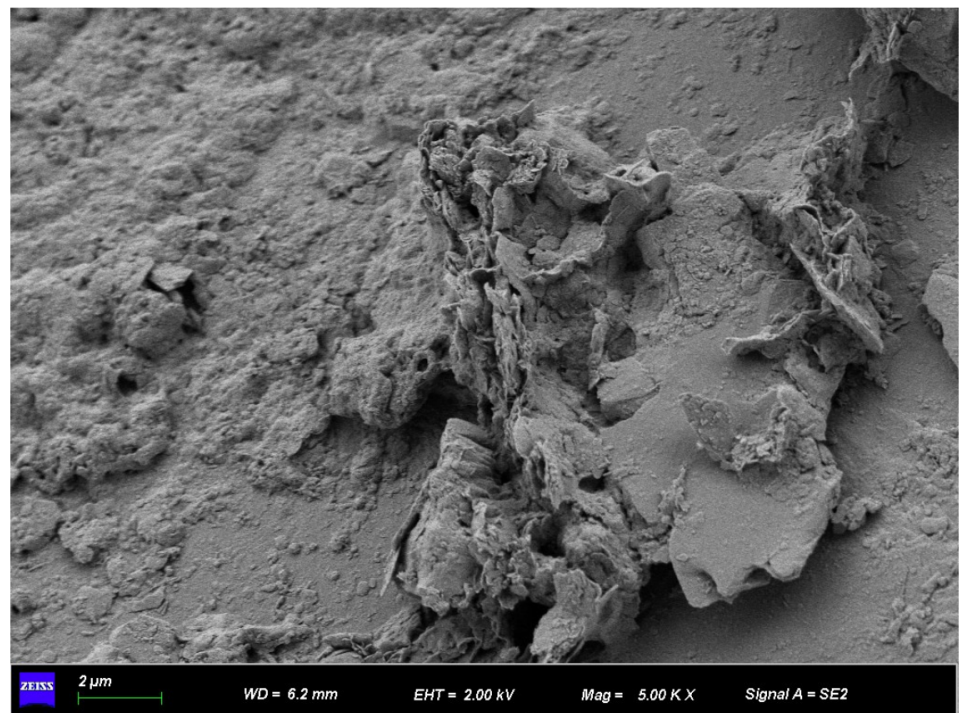


(b)

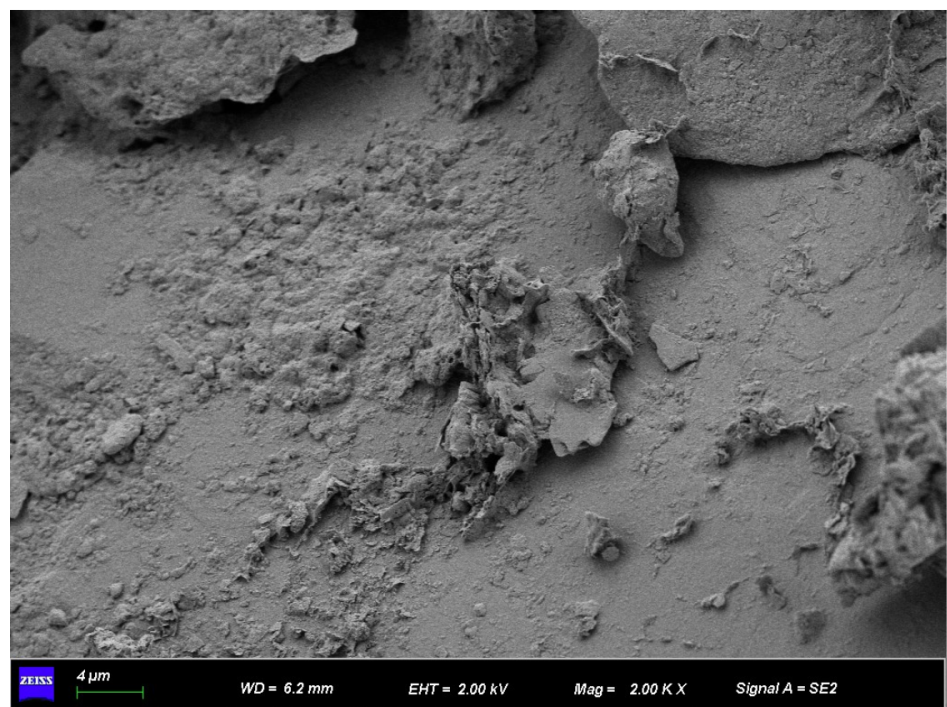


(c)

Figure 10. SEM micrographs of D1 at different magnifications. (a) 2 μm; (b) 4 μm; (c) 10 μm.

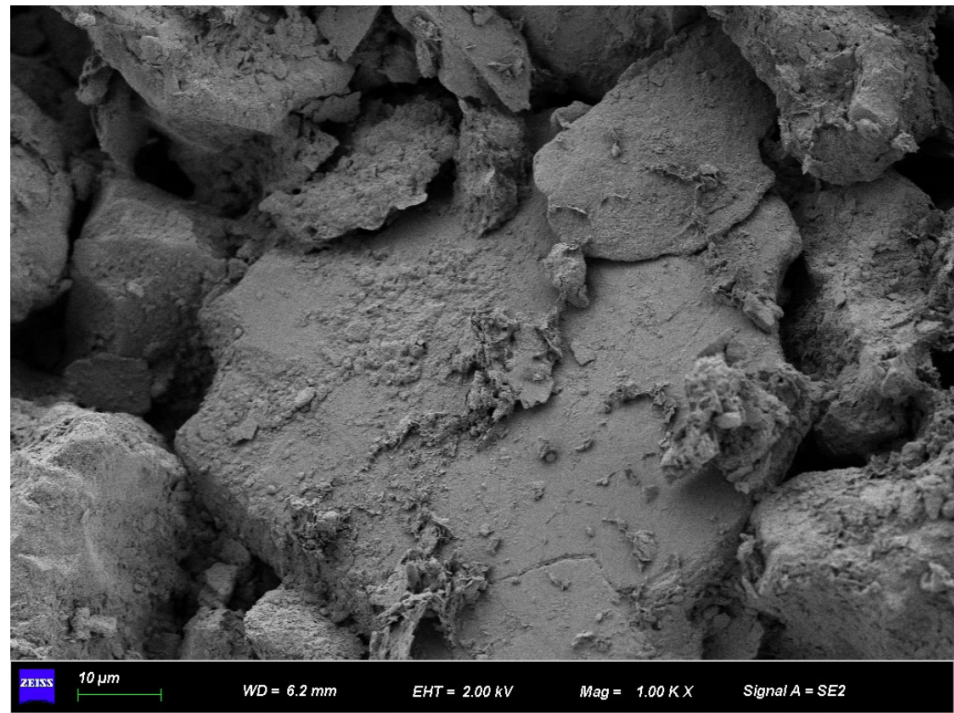


(a)



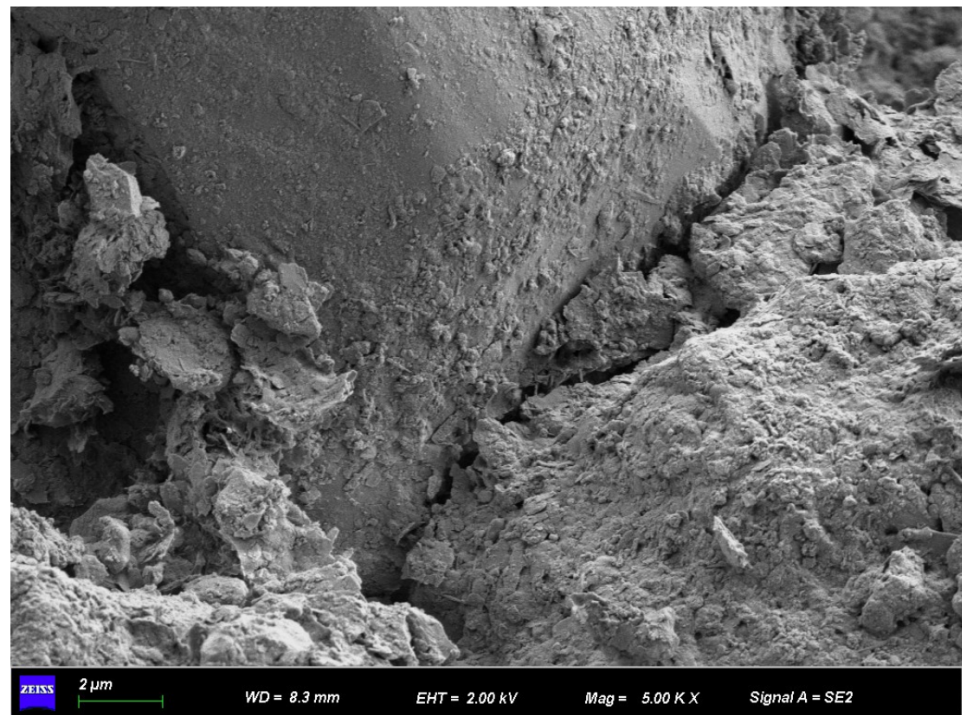
(b)

Figure 11. Cont.



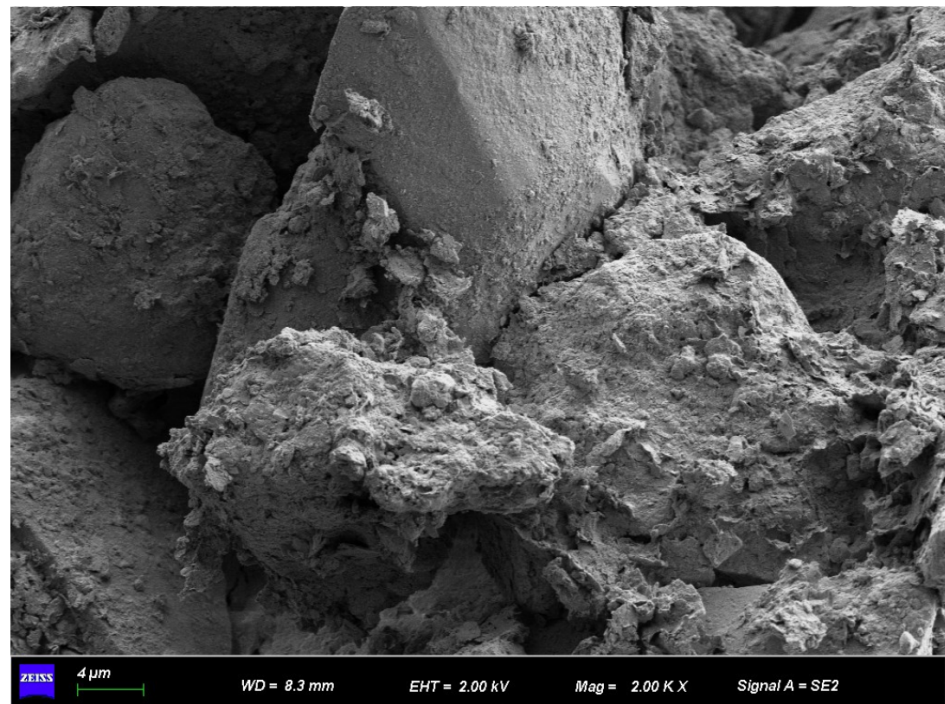
(c)

Figure 11. SEM micrographs of B3 at different magnifications. (a) 2 μm; (b) 4 μm; (c) 10 μm.

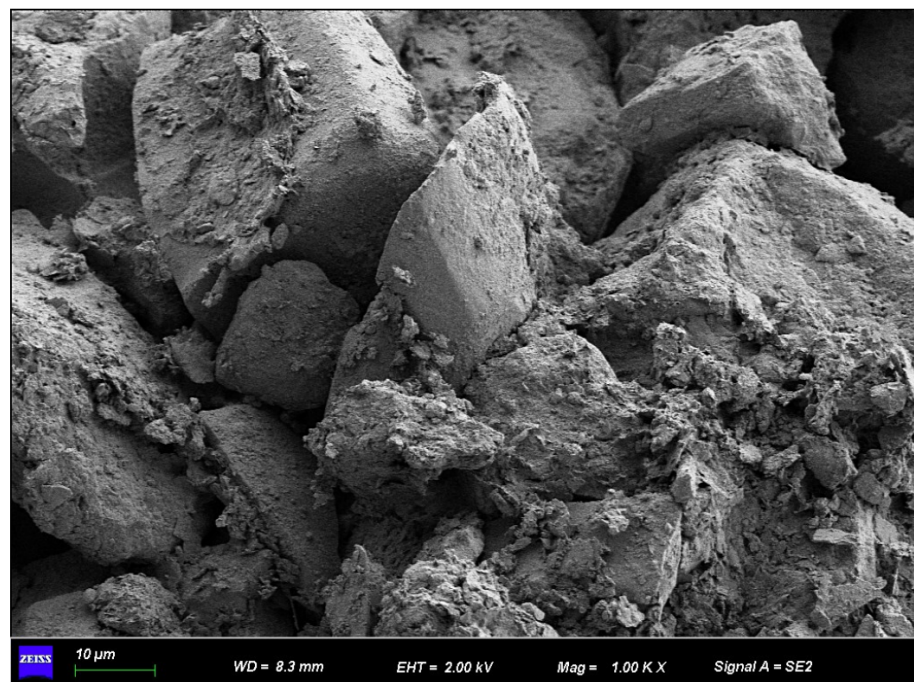


(a)

Figure 12. Cont.

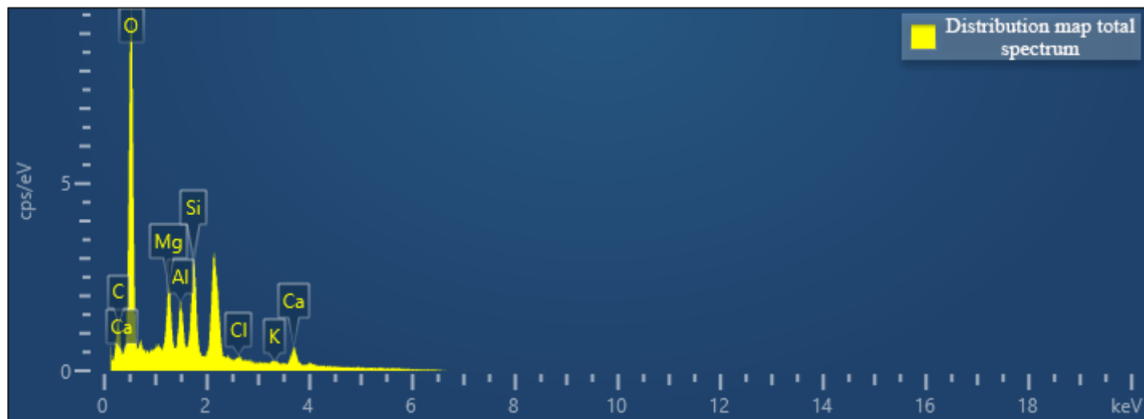


(b)

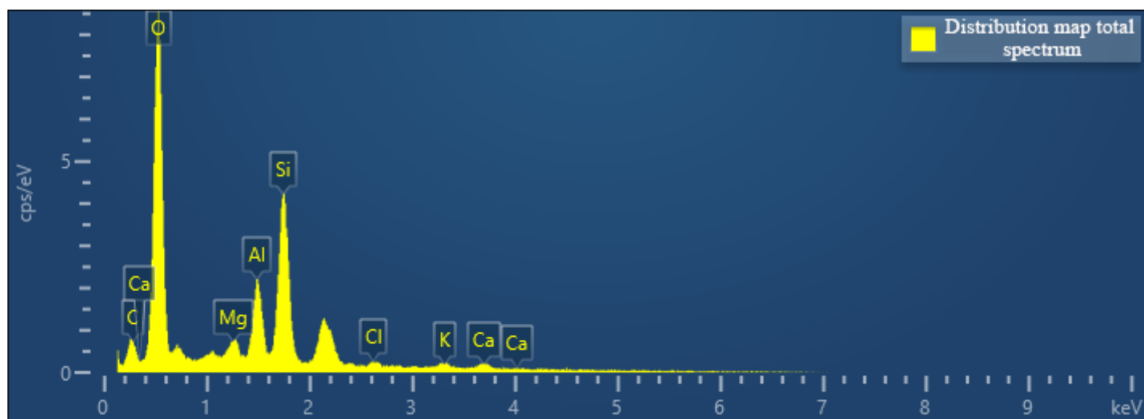


(c)

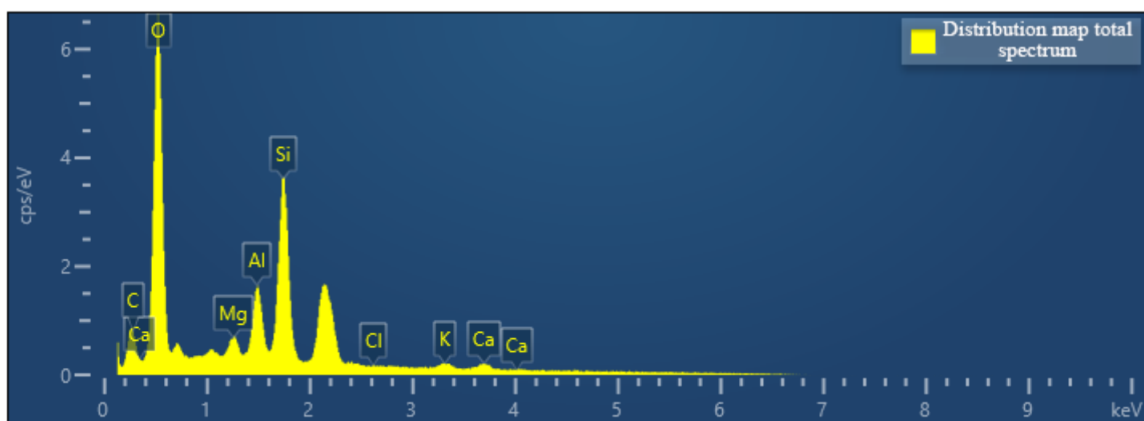
Figure 12. SEM micrographs of the blank control group at different magnifications. (a) 2 μm; (b) 4 μm; (c) 10 μm.



(a)



(b)



(c)

Figure 13. Element distribution of different soil–rock mixture columns. (a) D1; (b) B3; (c) Blank control group.

From the detection results of XRD (Figure 14, Table 3), it can be observed that the three groups of samples have the highest dolomite content, and the dolomite content of D1, B3, and the blank control group is 46.3%, 30%, and 18.7%, respectively. The calcite content is 2.9%, 3.1%, and 3.7%, respectively. Calcium ion is an important constituent element of dolomite and calcite, both of which exist in the form of calcium carbonate. The sum of the content of the two phases can also be regarded as the total content of calcium

carbonate crystals generated under the action of microbial mineralization. According to Table 3, the calcium carbonate content of the three groups of samples under the action of cementation is as follows: D1 > B3 > blank control group. Combined with the EDS composition analysis results of D1 and B3, the percentage of calcium ions in the sample D1 > B3, it is proved that in the whole process of microbial mineralization, D1 produces more calcium carbonate than B3, with better cementation performance, filling the pores between particles. The compressive capacity of the soil–rock mixture sample is stronger, which is consistent with the mechanical test results. At the same time, it also shows that calcium carbonate is indeed generated under the action of bacterial liquid and cementation reagent, which strengthens the internal connection between soil and rock, fills pores, and increases the strength of the sample. It can be seen that microbial mineralization technology can effectively strengthen the adhesion between soil particles. The SEM and XRD test results prove that *Sporosarcina pasteurii* can effectively induce the formation of calcium carbonate and generate crystals in the pores of particles to improve the mechanical properties of soil.

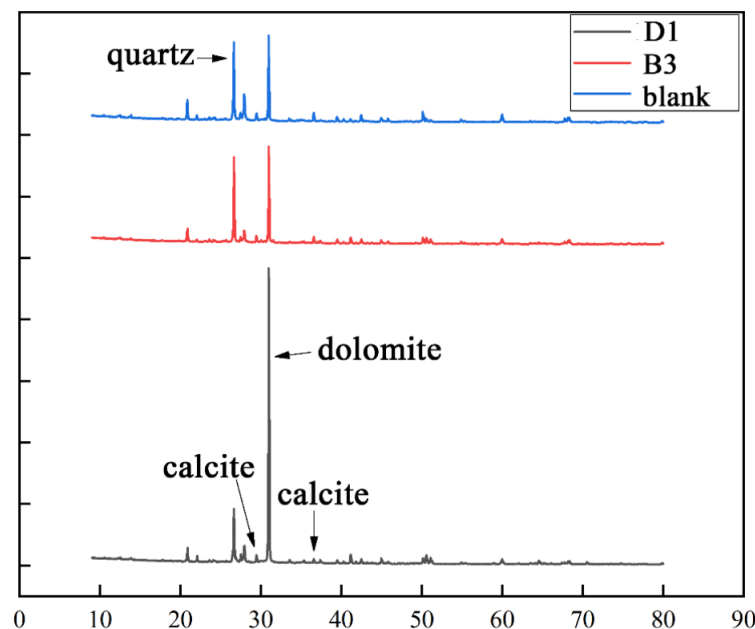


Figure 14. XRD pattern of the sample.

Table 3. Analysis results of various substances in MICP-treated samples.

Phase Name	Chemical Formula	Sample (Phase Content, Weight Percentage, wt%)		
		B3	D1	Blank
Illite	$KAl_2Si_3AlO_{10}(OH)_2$	8.8%	7.6%	8.3%
Kaolinite	$Al_4(OH)_8Si_4O_{10}$	0.9%	0.6%	0.6%
Quartz	SiO_2	33.0%	20.3%	30.2%
Microcline Feldspar	$KAlSi_3O_8$	5.8%	4.0%	6.0%
Albite	$NaAlSi_3O_8$	11.4%	13.9%	20.0%
Chlorite	$(MgFe)_6(SiAl)_4O_{10}(OH)_8$	6.2%	3.2%	8.9%
Calcite	$CaCO_3$	3.1%	2.9%	3.7%
Dolomite	$CaMgCO_3$	30.0%	46.3%	18.7%
Amphibole	$Al_{3.2} Ca_{3.4} Fe_{4.02} K_{0.6} Mg_6 Na Si_{12.8} O_{44} (OH)_4$	0.8%	1.2%	3.6%

4. Conclusions

A new exploration of the MICP curing method was carried out. The soil and rock with different rock block proportions and different rock particle sizes were proportioned, and the bacteria liquid and the cementing liquid were directly mixed by stirring and mixing method. The samples were prepared by stirring in the soil and rock, and then the

unconfined compressive strength mechanical test was carried out on the samples to test the optimal proportion of soil–rock mixture consolidation. The mineralization and cementation ability and physical and mechanical properties of the soil–rock mixture under the influence of rock content and particle size were discussed. The main conclusions are as follows:

- The soil–rock mixture is not a uniform carrier of the medium, and the stress on the surface of the sample is uneven. With the increase in the stress load, the stress–strain curve shows a zigzag upward trend and peak value;
- The cementation ability of soil and rock is related to the pore size between soil and rock. When the rock particle size is the same, the higher the proportion of block stone is, and the more pores between soil and rock particles, which is conducive to microbial cementation and mineralization and improves the sample strength;
- When the rock content is low, the difference between the particle size ratio of small-size rock and the particle size of soil is relatively small, which makes it easier to cement with a bacterial solution to form a block, enhancing the compressive capacity of soil and rock mass. When the rock content is high, the particle size difference of large rock soil particles is large, the pore space is large, and the oxygen is sufficient. At the same time, the large particle size rock has more particle contact points than the small particle size rock, so its unconfined compressive strength is large. When the rock content is the same, the pore space of the soil–rock mixture mixed with large-diameter boulders is larger than that of the soil–rock mixture containing small particles. When the sample is compressed, the pore space inside the sample mixed with large boulders is first destroyed, and the maximum bearing capacity of the small boulder soil–rock mixture is faster than that of the small boulders;
- When the rock content is 20–50%, the unconfined compressive strength decreases with the increase in particle size. When the rock block proportion is 60%, the value of unconfined compressive strength first decreases and then increases with the increase in particle size. In the samples with a low proportion of rock blocks, the overall force is more inclined to the nature of silt. In the process of compression, the pores between particles are destroyed. Due to the shrinkage of pores, the bound water increases, and the binding strength between particles decreases, making them easier to be destroyed;
- Among the soil–rock mixture samples, the unconfined compressive strength of the microbially cemented soil–rock mixture with particle size of 0.2–0.4 cm and 0.4–0.6 cm reaches the highest at 50% rock block proportion. The unconfined compressive strength of the microbially cemented soil–rock mixture with a rock particle size of 0.6–0.9 cm reaches the highest at 60% rock block proportion;
- Microbial mineralization technology can effectively strengthen the adhesion between soil and rock particles. Both SEM and XRD test results proved that *Sporosarcina pasteurii* could effectively induce the formation of calcium carbonate, and crystals are formed at the pores of the particles to improve the mechanical properties of the soil. Small particles of rocks are combined with silt, the cementation effect is better under the action of microbial mineralization, and the content of calcium carbonate crystals generated is higher than the crystals generated by large particles and silt under the action of mineralization.

Author Contributions: Methodology, J.L.; Formal analysis, Y.T. and J.L.; Investigation, Y.T.; Resources, G.W.; Data curation, Y.T.; Writing—original draft, Y.S.; Writing—review & editing, Y.S.; Visualization, Y.T.; Supervision, G.W.; Project administration, J.L. and G.W. All authors have read and agreed to the published version of the manuscript.

Funding: This work is supported by the Beijing Natural Science Foundation (8214060) and the National Natural Science Foundation of China (42107164).

Institutional Review Board Statement: Not applicable.

Informed Consent Statement: Informed consent was obtained from all subjects involved in the study.

Data Availability Statement: All data that support the findings of this study are available from the corresponding author upon reasonable request.

Conflicts of Interest: The authors declare that they have no conflict of interest to report regarding the present study.

References

1. Medley, E.; Goodman, R.E. Estimating the block volumetric proportions of melanges and similar block-in-matrix rocks (bim-rocks). In Proceedings of the 1st North American Rock Mechanics Symposium, Austin, TX, USA, 1–3 June 1994.
2. Yang, G.-Q.; Liu, H.; Zhou, Y.-T.; Xiong, B.-L. Post-construction performance of a two-tiered geogrid reinforced soil wall backfilled with soil-rock mixture. *Geotext. Geomembr.* **2014**, *42*, 91–97. [[CrossRef](#)]
3. Zhang, Z.-L.; Xu, W.-J.; Xia, W.; Zhang, H.-Y. Large-scale in-situ test for mechanical characterization of soil–rock mixture used in an embankment dam. *Int. J. Rock Mech. Min. Sci.* **2016**, *86*, 317–322. [[CrossRef](#)]
4. Fan, J.; Wang, D.; Qian, D. Soil-cement mixture properties and design considerations for reinforced excavation. *J. Rock Mech. Geotech. Eng.* **2018**, *10*, 791–797. [[CrossRef](#)]
5. Zhang, F.; Liu, Z.; Chen, Y.; Chen, L.; Huang, X.; Bai, Y.; Shi, C.; Zhou, T. Numerical simulation of mutually embedded settlement in miscellaneous fill. *Adv. Civ. Eng.* **2020**. [[CrossRef](#)]
6. Ptilakis, D.; Anastasiadis, A.; Vratsikidis, A.; Kapouniaris, A.; Massimino, M.R.; Abate, G.; Corsico, S. Large-scale field testing of geotechnical seismic isolation of structures using gravel-rubber mixtures. *Earthq. Eng. Struct. Dyn.* **2021**, *50*, 2712–2731. [[CrossRef](#)]
7. Yang, Z.; Li, S.; Jiang, Y.; Hu, Y.; Liu, X. Shear Mechanical Properties of the Interphase between Soil–Rock Mixtures and Bench Bedrock Slope Surfaces. *Int. J. Géoméch.* **2022**, *22*, 04022047. [[CrossRef](#)]
8. Kai, C.; Xiang, J. Effect of coarse grain content on the dynamic shear modulus and damping ratio of mixed soil under seismic load in western Sichuan. *China J. Highw. Transp.* **2019**, *32*, 123.
9. Ji, X.; Han, B.; Hu, J.; Li, S.; Xiong, Y.; Sun, E. Application of the discrete element method and CT scanning to investigate the compaction characteristics of the soil–rock mixture in the subgrade. *Road Mater. Pavement Des.* **2020**, *23*, 397–413. [[CrossRef](#)]
10. Imran, A.; Nakashima, K.; Evelpidou, N.; Kawasaki, S. Durability Improvement of Biocemented Sand by Fiber-Reinforced MICP for Coastal Erosion Protection. *Materials* **2022**, *15*, 2389. [[CrossRef](#)]
11. Tsai, C.-P.; Ye, J.-H.; Ko, C.-H.; Lin, Y.-R. An Experimental Investigation of Microbial-Induced Carbonate Precipitation on Mitigating Beach Erosion. *Sustainability* **2022**, *14*, 2513. [[CrossRef](#)]
12. Wang, X.; Li, C.; He, J. A highly effective strain screened from soil and applied in cementing fine sand based on MICP-bonding technology. *J. Biotechnol.* **2022**, *350*, 55–66. [[CrossRef](#)] [[PubMed](#)]
13. Zhang, J.; Shi, X.; Chen, X.; Huo, X.; Yu, Z. Microbial-Induced Carbonate Precipitation: A Review on Influencing Factors and Applications. *Adv. Civ. Eng.* **2021**, *2021*, 1–16. [[CrossRef](#)]
14. Leeprasert, L.; Chonudomkul, D.; Boonmak, C. Biocalcifying Potential of Ureolytic Bacteria Isolated from Soil for Biocementation and Material Crack Repair. *Microorganisms* **2022**, *10*, 963. [[CrossRef](#)] [[PubMed](#)]
15. Wang, Y.; Wang, G.; Wan, Y.; Yu, X.; Zhao, J.; Shao, J. Recycling of dredged river silt reinforced by an eco-friendly technology as microbial induced calcium carbonate precipitation (MICP). *Soils Found.* **2022**, *62*, 101216. [[CrossRef](#)]
16. Liu, P.; Shao, G.; Huang, R. Mechanical Properties and constitutive model of MICP-cemented sand. *J. Southeast Univ. Nat. Sci. Ed.* **2019**, *49*, 720–726.
17. Zhao, Y.; Wang, Q.; Yuan, M.; Chen, X.; Xiao, Z.; Hao, X.; Zhang, J.; Tang, Q. The Effect of MICP on Physical and Mechanical Properties of Silt with Different Fine Particle Content and Pore Ratio. *Appl. Sci.* **2021**, *12*, 139. [[CrossRef](#)]
18. Mukherjee, S.; Sahu, R.B.; Mukherjee, J. Effect of Biologically Induced Cementation via Ureolysis in Stabilization of Silty Soil. *Geomicrobiol. J.* **2021**, *39*, 66–82. [[CrossRef](#)]
19. Shen, T.; Wang, S.; Xue, L.; Li, X.; He, B. An experimental study of sandy clayey purple soil enhanced through microbial-induced calcite precipitation. *Rock Soil Mech.* **2019**, *40*, 3115–3124.
20. Liu, X.; Pan, C.; Yu, J.; Fan, J. Study on Micro-Characteristics of Microbe-Induced Calcium Carbonate Solidified Loess. *Crystals* **2021**, *11*, 1492. [[CrossRef](#)]
21. Liu, X.-J.; Fan, J.-Y.; Yu, J.; Gao, X. Solidification of loess using microbial induced carbonate precipitation. *J. Mt. Sci.* **2021**, *18*, 265–274. [[CrossRef](#)]
22. Ouyang, Q.; Xiao, H.; Li, Z.; Jiang, W.; Su, H.; Tian, X.; Ouyang, M. Experimental Study on the Influence of Microbial Content on Engineering Characteristics of Improved Expansive Soil. *Front. Earth Sci.* **2022**, *10*, 863357. [[CrossRef](#)]
23. Tian, X.; Xiao, H.; Li, Z.; Li, Z.; Su, H.; Ouyang, Q. Experimental Study on the Strength Characteristics of Expansive Soils Improved by the MICP Method. *Geofluids* **2022**, *2022*, 1–10. [[CrossRef](#)]
24. Yue, J.; Zhao, L.; Zhang, B.; Kong, Q.; Wang, S.; Wang, H. Effect of Glutinous Rice Slurry on the Reinforcement of Silt in the Yellow River Basin by Microbially Induced Carbonate Precipitation (MICP): Mechanical Property and Microcosmic Structure. *Adv. Mater. Sci. Eng.* **2021**, *2021*, 1–23. [[CrossRef](#)]
25. Wang, Y.; Wang, G.; Zhong, Y.; Shao, J.; Zhao, J.; Li, D. Comparison of different treatment methods on macro-micro characteristics of Yellow River silt solidified by MICP technology. *Mar. Georesources Geotechnol.* **2022**, 1–11. [[CrossRef](#)]

26. Wang, X.; Wang, X.; Shen, J.; Zhu, C. Particle size and confining-pressure effects of shear characteristics of coral sand: An experimental study. *Bull. Eng. Geol. Environ.* **2022**, *81*, 97. [[CrossRef](#)]
27. Wang, X.; Wang, Y.; Liao, C.; Cui, J.; Shen, J.-H.; Wang, X.-Z.; Zhu, C.-Q. Particle breakage mechanism and particle shape evolution of calcareous sand under impact loading. *Bull. Eng. Geol. Environ.* **2022**, *81*, 372. [[CrossRef](#)]
28. Chen, M.; Li, Y.; Jiang, X.; Zhao, D.; Liu, X.; Zhou, J.; He, Z.; Zheng, C.; Pan, X. Study on soil physical structure after the bioremediation of Pb pollution using microbial-induced carbonate precipitation methodology. *J. Hazard. Mater.* **2021**, *411*, 125103. [[CrossRef](#)]
29. Chen, P.; Zheng, H.; Xu, H.; Gao, Y.-X.; Ding, X.-Q.; Ma, M.-L. Microbial induced solidification and stabilization of municipal solid waste incineration fly ash with high alkalinity and heavy metal toxicity. *PLoS ONE* **2019**, *14*, e0223900. [[CrossRef](#)]
30. Chen, X.; Zhang, D.; Larson, S.L.; Ballard, J.H.; Knotek-Smith, H.M.; Nie, J.; Hu, N.; Ding, D.; Han, F.X. Microbially Induced Carbonate Precipitation Techniques for the Remediation of Heavy Metal and Trace Element-Polluted Soils and Water. *Water Air Soil Pollut.* **2021**, *232*, 1–15. [[CrossRef](#)]
31. He, J.; Chen, X.; Zhang, Q.; Achal, V. More effective immobilization of divalent lead than hexavalent chromium through carbonate mineralization by *Staphylococcus epidermidis* HJ2. *Int. Biodeterior. Biodegrad.* **2019**, *140*, 67–71. [[CrossRef](#)]
32. Kang, B.; Zha, F.; Deng, W.; Wang, R.; Sun, X.; Lu, Z. Biocementation of Pyrite Tailings Using Microbially Induced Calcite Carbonate Precipitation. *Molecules* **2022**, *27*, 3608. [[CrossRef](#)] [[PubMed](#)]
33. Kang, B.; Zha, F.; Li, H.; Xu, L.; Sun, X.; Lu, Z. Bio-Mediated Method for Immobilizing Copper Tailings Sand Contaminated with Multiple Heavy Metals. *Crystals* **2022**, *12*, 522. [[CrossRef](#)]
34. Kim, J.-H.; Lee, J.-Y. An optimum condition of MICP indigenous bacteria with contaminated wastes of heavy metal. *J. Mater. Cycles Waste Manag.* **2018**, *21*, 239–247. [[CrossRef](#)]
35. Torres-Aravena, E.; Duarte-Nass, C.; Azócar, L.; Mella-Herrera, R.; Rivas, M.; Jeison, D. Can Microbially Induced Calcite Precipitation (MICP) through a Ureolytic Pathway be Successfully Applied for Removing Heavy Metals from Wastewaters? *Crystals* **2018**, *8*, 438. [[CrossRef](#)]
36. Zha, F.; Wang, H.; Kang, B.; Liu, C.; Xu, L.; Tan, X. Improving the Strength and Leaching Characteristics of Pb-Contaminated Silt through MICP. *Crystals* **2021**, *11*, 1303. [[CrossRef](#)]
37. Badiiee, H.; Sabermahani, M.; Javadi, A.S.; Bouazza, A. Comparison of Microbially Induced Carbonate Precipitation with Ordinary Portland Cement Producing Macroporous Pervious Concrete. *J. Mater. Civ. Eng.* **2021**, *33*, 04021070. [[CrossRef](#)]
38. Castro-Alonso, M.J.; Montañez-Hernandez, L.E.; Sanchez-Muñoz, M.A.; Macias Franco, M.R.; Narayanasamy, R.; Balagurusamy, N. Microbially Induced Calcium Carbonate Precipitation (MICP) and Its Potential in Bioconcrete: Microbiological and Molecular Concepts. *Front. Mater.* **2019**, *6*, 126. [[CrossRef](#)]
39. Feng, C.; Cui, B.; Ge, H.; Huang, Y.; Zhang, W.; Zhu, J. Reinforcement of Recycled Aggregate by Microbial-Induced Mineralization and Deposition of Calcium Carbonate—Influencing Factors, Mechanism and Effect of Reinforcement. *Crystals* **2021**, *11*, 887. [[CrossRef](#)]
40. Lee, Y.S.; Park, W. Current challenges and future directions for bacterial self-healing concrete. *Appl. Microbiol. Biotechnol.* **2018**, *102*, 3059–3070. [[CrossRef](#)]
41. Lin, H.; Suleiman, M.T.; Jabbour, H.M.; Brown, D.G. Bio-grouting to enhance axial pull-out response of pervious concrete ground improvement piles. *Can. Geotech. J.* **2018**, *55*, 119–130. [[CrossRef](#)]
42. Mondal, S.; Ghosh, A. Review on microbial induced calcite precipitation mechanisms leading to bacterial selection for microbial concrete. *Constr. Build. Mater.* **2019**, *225*, 67–75. [[CrossRef](#)]
43. Zhao, Y.; Peng, L.; Zeng, W.; Poon, C.S.; Lu, Z. Improvement in properties of concrete with modified RCA by microbial induced carbonate precipitation. *Cem. Concr. Compos.* **2021**, *124*, 104251. [[CrossRef](#)]
44. Cheng, Y.-J.; Tang, C.-S.; Pan, X.-H.; Liu, B.; Xie, Y.-H.; Cheng, Q.; Shi, B. Application of microbial induced carbonate precipitation for loess surface erosion control. *Eng. Geol.* **2021**, *294*, 106387. [[CrossRef](#)]
45. Chung, H.; Kim, S.H.; Nam, K. Application of microbially induced calcite precipitation to prevent soil loss by rainfall: Effect of particle size and organic matter content. *J. Soils Sediments* **2020**, *21*, 2744–2754. [[CrossRef](#)]
46. Gao, Y.; Tang, X.; Chu, J.; He, J. Microbially Induced Calcite Precipitation for Seepage Control in Sandy Soil. *Geomicrobiol. J.* **2019**, *36*, 366–375. [[CrossRef](#)]
47. Gomez, M.G.; DeJong, J.T.; Anderson, C.M. Effect of bio-cementation on geophysical and cone penetration measurements in sands. *Can. Geotech. J.* **2018**, *55*, 1632–1646. [[CrossRef](#)]
48. Nikseresht, F.; Landi, A.; Sayyad, G.; Ghezlbash, G.; Schulin, R. Sugarcane molasse and vinasse added as microbial growth substrates increase calcium carbonate content, surface stability and resistance against wind erosion of desert soils. *J. Environ. Manag.* **2020**, *268*, 110639. [[CrossRef](#)]
49. Teng, F.; Sie, Y.-C.; Ouedraogo, C. Strength improvement in silty clay by microbial-induced calcite precipitation. *Bull. Eng. Geol. Environ.* **2021**, *80*, 6359–6371. [[CrossRef](#)]
50. Zamani, A.; Xiao, P.; Baumer, T.; Carey, T.J.; Sawyer, B.; DeJong, J.T.; Boulanger, R.W. Mitigation of Liquefaction Triggering and Foundation Settlement by MICP Treatment. *J. Geotech. Geoenvironmental Eng.* **2021**, *147*, 04021099. [[CrossRef](#)]
51. Zhang, J.; Li, C.; Wang, S.; Bai, S. Three-Dimensional Reconstruction of Biomineralized Sand and Particle-Flow-Code Numerical Simulation of Penetration Resistance Characteristics of Biomineralization Crust. *Int. J. Géoméché.* **2021**, *21*, 04021048. [[CrossRef](#)]

52. Cardoso, R.; Pires, I.; Duarte, S.O.; Monteiro, G.A. Effects of clay's chemical interactions on biocementation. *Appl. Clay Sci.* **2018**, *156*, 96–103. [\[CrossRef\]](#)
53. Cheshomi, A.; Mansouri, S. Study the grain size and infiltration method effects for sand soil improvement using the microbial method. *Geomicrobiol. J.* **2019**, *37*, 355–365. [\[CrossRef\]](#)
54. Konstantinou, C.; Biscontin, G.; Jiang, N.-J.; Soga, K. Application of microbially induced carbonate precipitation to form bio-cemented artificial sandstone. *J. Rock Mech. Geotech. Eng.* **2021**, *13*, 579–592. [\[CrossRef\]](#)
55. Oualha, M.; Bibi, S.; Sulaiman, M.; Zouari, N. Microbially induced calcite precipitation in calcareous soils by endogenous *Bacillus cereus*, at high pH and harsh weather. *J. Environ. Manag.* **2020**, *257*, 109965. [\[CrossRef\]](#) [\[PubMed\]](#)
56. Tang, C.-S.; Yin, L.-Y.; Jiang, N.-J.; Zhu, C.; Zeng, H.; Li, H.; Shi, B. Factors affecting the performance of microbial-induced carbonate precipitation (MICP) treated soil: A review. *Environ. Earth Sci.* **2020**, *79*, 94. [\[CrossRef\]](#)
57. Terzis, D.; Laloui, L. Cell-free soil bio-cementation with strength, dilatancy and fabric characterization. *Acta Geotech.* **2019**, *14*, 639–656. [\[CrossRef\]](#)
58. Tian, Z.; Tang, X.; Li, J.; Xiu, Z.; Xue, Z. Influence of the Grouting Parameters on Microbially Induced Carbonate Precipitation for Soil Stabilization. *Geomicrobiol. J.* **2021**, *38*, 755–767. [\[CrossRef\]](#)
59. Cardoso, R.; Pedreira, R.; Duarte, S.O.; Monteiro, G.A. About calcium carbonate precipitation on sand biocementation. *Eng. Geol.* **2020**, *271*, 105612. [\[CrossRef\]](#)
60. Jin, G.; Xu, K.; Xu, C.; Huang, M.; Qasem, R.G.A.; Guo, S.; Liu, S. Cementation of Shale Soils by MICP Technology and Its Damage Characteristics Due to Freeze–Thaw Weathering Processes. *J. Cold Reg. Eng.* **2020**, *34*, 04020023. [\[CrossRef\]](#)
61. Martinez, A.; Huang, L.; Gomez, M.G.; Terzis, D.; Bernier-Latmani, R.; Laloui, L.; Haigh, S.; Nguyen, V.T.; Heindl, H.; Pereira, J.M.; et al. Thermal conductivity of MICP-treated sands at varying degrees of saturation. *Geotech. Lett.* **2019**, *9*, 15–21. [\[CrossRef\]](#)
62. Xiao, Y.; Ma, G.; Wu, H.; Lu, H.; Zaman, M. Rainfall-Induced Erosion of Biocemented Graded Slopes. *Int. J. Géoméch.* **2022**, *22*, 04021256. [\[CrossRef\]](#)
63. Xiao, Y.; Tang, Y.; Ma, G.; McCartney, J.S.; Chu, J. Thermal Conductivity of Biocemented Graded Sands. *J. Geotech. Geoenvironmental Eng.* **2021**, *147*, 04021106. [\[CrossRef\]](#)
64. Chen, H.-J.; Tsai, T.-M.; Wu, C.-H. Research on the feasibility of strengthening the soil structure by biomineralization. *J. Chin. Inst. Eng.* **2021**, *44*, 214–222. [\[CrossRef\]](#)
65. Nafisi, A.; Liu, Q.; Montoya, B.M. Effect of stress path on the shear response of bio-cemented sands. *Acta Geotech.* **2021**, *16*, 3239–3251. [\[CrossRef\]](#)
66. Shih, D.-S.; Lai, T.-Y.; Hsu, Z.-M. Applying Biomineralization Technology to Study the Effects of Rainfall Induced Soil Erosion. *Water* **2019**, *11*, 2555. [\[CrossRef\]](#)
67. Xiao, P.; Liu, H.; Stuedlein, A.W.; Evans, T.M.; Xiao, Y. Effect of relative density and biocementation on cyclic response of calcareous sand. *Can. Geotech. J.* **2019**, *56*, 1849–1862. [\[CrossRef\]](#)
68. Zamani, A.; Montoya, B.M. Undrained Monotonic Shear Response of MICP-Treated Silty Sands. *J. Geotech. Geoenvironmental Eng.* **2018**, *144*, 0401802. [\[CrossRef\]](#)
69. Zamani, A.; Montoya, B.M. Undrained cyclic response of silty sands improved by microbial induced calcium carbonate precipitation. *Soil Dyn. Earthq. Eng.* **2019**, *120*, 436–448. [\[CrossRef\]](#)
70. Whiffin, V.S.; van Paassen, L.; Harkes, M.P. Microbial Carbonate Precipitation as a Soil Improvement Technique. *Geomicrobiol. J.* **2007**, *24*, 417–423. [\[CrossRef\]](#)
71. DeJong, J.T.; Fritzges, M.B.; Nüsslein, K. Microbially Induced Cementation to Control Sand Response to Undrained Shear. *J. Geotech. Geoenvironmental Eng.* **2006**, *132*, 1381–1392. [\[CrossRef\]](#)
72. Ramachandran, S.K.; Ramakrishnan, V.; Bang, S.S. Remediation of concrete using micro-organisms. *ACI Mater. J. Am. Concr. Inst.* **2001**, *98*, 3–9.
73. Research Institute of Highway Science, Ministry of Communications. *Test Methods of Soils for Highway Engineering*; JTG E40-2007, 428P, A424; Highway Science Research Institute of the Ministry of Communications: Beijing, China, 2007.
74. Yang, Z.; Li, J.; Jiang, Y.; Hu, Y.; Zhao, Y. Influence of stone content on shear mechanical properties of soil-rock mixture-bedrock interface. *J. Geotech. Eng.* **2021**, *43*, 1443–1452.

Disclaimer/Publisher's Note: The statements, opinions and data contained in all publications are solely those of the individual author(s) and contributor(s) and not of MDPI and/or the editor(s). MDPI and/or the editor(s) disclaim responsibility for any injury to people or property resulting from any ideas, methods, instructions or products referred to in the content.